Pergamon

Int. J. Impact Engng, Vol. 17, pp. 253–262, 1995
Elsevier Science Ltd
Printed in Great Britain
0734-743X/95 $9.50+0.00

THE IMPACT OF PERIODIC COMET SHOEMAKER-LEVY 9 ON JUPITER*

D. A. Crawford, M. B. Boslough, T. G. Trucano and A. C. Robinson

Sandia National Laboratories, Albuquerque, NM 87185-0821

Summary—We have performed computational shock-physics simulations of the hypervelocity (60 km/s) impact of 1-3 km, water-ice spheres entering a hydrogen-helium Jovian atmosphere, conditions that simulate current estimates for the collision of fragments of Periodic Comet Shoemaker-Levy 9 with Jupiter. Observatories in space and around the world observed the events as they occurred in July, 1994. The Hubble Space Telescope obtained high resolution images of the impact-generated fireballs that appeared above the limb of Jupiter and of the visibly dark ejecta patterns distributed over broad regions of the Jovian stratosphere. Time-resolved radiometric measurements from spacecraft and Earth-based observatories detected multiple arrivals for each impact: the entry flash as the incoming fragment entered the atmosphere, arrival of the debris front (fireball) as it emerged above the Jovian limb (which varies as a function of wavelength), the arrival of the debris front into sunlight and finally, the emergence of the impact site as it rotated into view. We used the Eulerian shock-physics code CTH, and its parallel version PCTH to perform 2-D analyses of penetration and breakup, and 3-D analyses of the growth of the resulting fireball during the first 120 seconds after fragment entry. For sufficiently large fragments, impact-generated fireballs rise into line-of-sight over the Jovian limb. For 1- and 3-km fragments impacting 6° beyond the limb, this occurs approximately 75 and 50 seconds after impact, respectively. Measurement of the time interval between fragment entry and limb arrival provides information that places strong restrictions on equivalent explosive yield (from which fragment mass can be estimated). Measurements of more arrivals help constrain the effective penetration depth, thereby lending insight into the material and mechanical properties of the cometary fragments. We believe that matching high resolution imagery and time-resolved photometry with numerical simulations will provide some of the best means by which Shoemaker-Levy 9 fragment masses and material properties will be determined.

INTRODUCTION

In early July, 1992, periodic comet Shoemaker-Levy 9 broke up during a close encounter with Jupiter. For a brief two year period, about 20 large fragments and associated debris followed one last orbit about Jupiter before striking the planet at an estimated velocity of 60 km/s. Most of the debris collided with the planet over a 2 month period centered on July, 1994, with the largest fragments colliding during July 16-22 (UT). Images obtained from the Hubble Space Telescope prior to the impacts placed an upper limit of 4 km on the diameter of the fragments [1], but it was widely felt that the fragments would be smaller [2,3]. The impact sites were located just beyond the limb of Jupiter (see Fig. 1) and were not directly visible from Earth; nevertheless, the Galileo, Voyager II and Ulysses spacecraft were positioned for direct viewing of the impact points. Although impact phenomena were not spatially resolved by the spacecraft, their timing, spectral and luminosity data will be invaluable for comparison with analytical and numerical models. Debris from the impacts were predicted to be visible in line-of-sight from Earth within seconds to minutes after the more energetic impacts [4-6] and the impact locations themselves were expected to rotate into

*This work was sponsored by the Department of Energy and the National Science Foundation and conducted at Sandia National Laboratories under the auspices of the Department of Energy under contract DE-AC04-94AL85000.

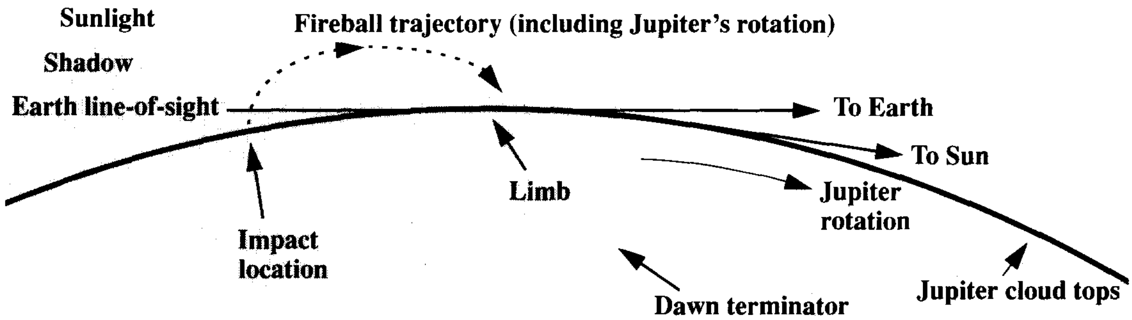

Fig. 1. Lateral view of the impact geometry. Impacts occured in darkness on the far side of Jupiter relative to Earth. Ballistic fireball/debris blown out by the explosive release of kinetic energy upon impact of some of the larger fragments first crossed into line-of-site with Earth and then into sunlight. After about 10-30 minutes, the debris fell back onto the stratosphere over a broad area, producing the large infrared signature and debris pattern seen by many observers. Modified from [6].

view within 7-20 minutes. Data collected from orbital-based, earth-based and airborne instruments confirmed this basic scenario. Measurements of optical flashes reflected off of Jupiter's moons were attempted but no observations had been confirmed as of September, 1994.

The purpose of modeling such an impact is twofold. First, the impacts will hopefully provide a means by which the hypervelocity impact community can assess highly energetic impacts (the kinetic energy of some fragments may have been as much as 10^7 MT equivalent) and validate the current generation of analytical models and shock physics codes [4-17]. Second, models such as this provide input for modeling the long-term response of the Jovian atmosphere [18-20] and predictions that guide astronomical observations and help to interpret the data.

The numerical simulations that we are presenting here are divided into two parts. The first part is a two dimensional simulation of the entry, deformation and breakup of the cometary fragments as they penetrate the Jovian atmosphere. These simulations are followed in some cases by the much more computationally intensive 3-D simulations of the generation and growth of the resulting fireballs.

ENTRY, DEFORMATION AND BREAKUP OF COMET FRAGMENTS IN THE JOVIAN ATMOSPHERE

We used the CTH Eulerian shock-physics code [21] to simulate two- and three-dimensional representations of the impact events. The 2-D computations are of the penetration phase, simulating the entry, deformation and breakup of the impacting comet fragments. The calculations are performed in a "reverse ballistic" sense using a Jovian atmosphere moving upward at 60 km/s impinging upon an initially stationary fragment (Fig. 2). The Eulerian mesh extends 100 km radially and 1000 km above and below the comet. The fragment is maintained in a high resolution portion of the mesh (equivalent to 25 computational zones across the projectile radius and extending 10 km vertically and 5 km radially) by Galilean transformations of the entire mesh every 0.1 seconds of simulation time. Zone size gradually increases away from the high resolution portion of the mesh (at a rate < 1.05x the neighboring zone) in order to preserve all the materials of the calculation yet maintain computational efficiency.

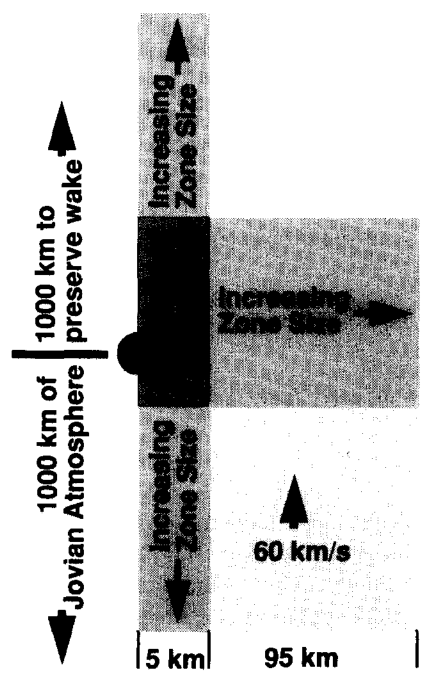

Fig. 2. Mesh geometry for two-dimensional impact/penetration simulations. Highest resolution portion of the mesh corresponds to 25 zones across the projectile radius (R25).

The comet fragment in the simulation is composed of water ice with initial density and temperature of 0.95 g/cm^3 and 100 K, respectively. For the ice, we used a tabularized version of the ANEOS equation-of-state which allows melting and vaporization [22]. We assume a Jovian atmospheric stratigra-

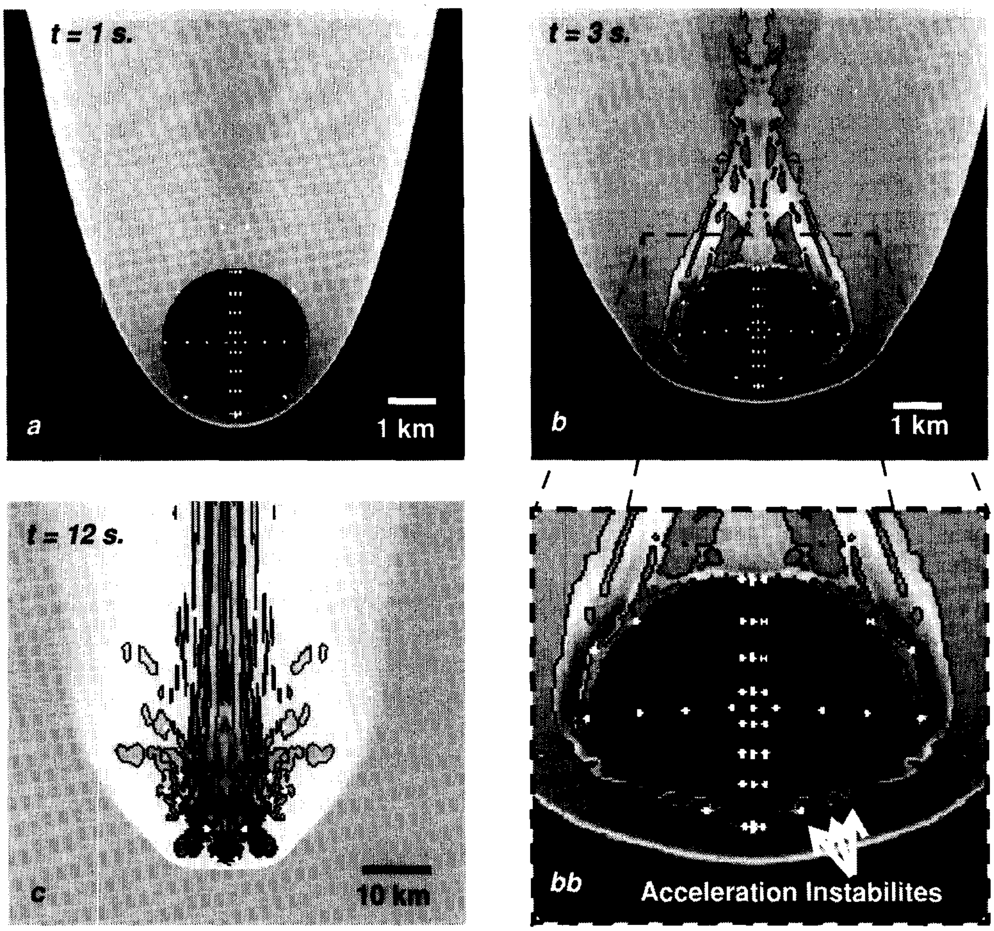

Fig. 3. Sequential stages of projectile entry (*a*), deformation (*b, bb*) and breakup (*c*). During entry (*a*), the projectile forms a clean bow shock in the upper reaches of the Jovian atmosphere. Atmospheric temperatures at the leading edge of the projectile reach values as great as 35,000 K. During deformation (*b*), the leading edge of the projectile flattens and Rayleigh-Taylor-like acceleration instabilities (*bb*) develop. These instabilities eventually lead to breakup (*c*) of the body.

phy that matches Voyager data at high altitudes (Orton, unpublished data) and extends adiabatically to lower altitudes. The atmosphere is assumed to consist of 89% hydrogen and 11% helium at all altitudes and is modeled with a tabular equation-of-state allowing dissociation and ionization [23]. It is scaled vertically by a factor of 1.41 to account for the approximate 45° entry angle and inserted into the lower portion of the computational mesh. The atmosphere propagates into the upper portion of the mesh as the comet deforms and breaks up in the higher-pressure regions of the lower atmosphere.

In Figure 3, we show the sequential stages of projectile entry, deformation and breakup of cometary fragments as they enter the Jovian atmosphere. During entry into the low density outermost reaches of the atmosphere, the projectile forms a clean bow shock. Atmospheric temperatures at the leading edge of the projectile reach values as great as 35,000 K. During deformation, the projectile thins and the leading edge flattens. Acceleration instabilities develop [24]. Eventually, projectile thinning meets with the growing instabilities and breakup occurs. During penetration, the projectile continuously gives up kinetic energy to heating and deflection of the Jovian atmosphere (a relatively small amount goes towards internal heating of the cometary constituents).

The total energy deposited by hypothetical 1-, 2- and 3-km diameter cometary fragments during their penetration of the Jovian atmosphere is shown in the plots of Figure 4. An important result evident in all of these calculations is that most of a large fragment's kinetic energy and mass will be deposited beneath Jupiter's outermost visible cloud layer which is about 10-15 km above the reference altitude at 1-bar. Because most of the fragment's mass is deposited at depth, less than 1% of the fragment mass is entrained in the upwardly growing fireball.

Figure 4a illustrates that mass is the governing parameter that determines the maximum penetration depth of the cometary fragments. A 1-km fully dense ice sphere penetrates only 130 km below the 1-bar level (here defined as 0 km altitude) whereas a 3-km fully dense ice sphere penetrates over 300 km below the 1-bar level. A porous 3-km impactor has the same maximum penetration depth as an equivalent mass 2-km impactor but has remarkably different overall energy deposition behavior. Not surprisingly, at high altitudes, where the projectile has not yet begun to deform and energy deposition is governed by cross-sectional area, its energy deposition behavior is similar to the fully dense 3-km impactor. As will be shown later, preliminary results from 3-D PCTH simulations suggest that fireballs that result from these types of comet-Jupiter impacts are sensitive to the nature of these energy deposition curves; hence, it may be possible to use measurements of fireball growth and evolution as a means of estimating the mass and material properties of the impacting fragments.

The importance of body shape (Fig. 4b) was investigated by performing simulations using a 2-D axisymmetric sphere, short rod and flat disk [7]. There is significant dependence on body shape. For consistency with other simulations, however, we will use spheres as representative of penetration behavior in this velocity and size regime. For the three shape-dependence simulations performed, the average penetration depth was 275±25 km below the 1-bar level for a body with mass equivalent to a 3 km sphere. Simulations using L/D=1 ice cylinders with yield strengths of 0, 10 and 100 bars were used to investigate the importance of yield strength on the overall penetration behavior (Fig. 4c). Predictably, low strength impactors yielded lower overall penetration behavior.

Sensitivity to the numerics was tested with three different numerical resolutions R10, R25 and R50, corresponding to 10, 25 and 50 computational zones across the radius of the projectile (Fig. 4d). Similar maximum penetration depths were seen for each case (with the higher resolution calculations penetrating slightly less). Although, significant differences were seen in the character of the energy deposition curves, sensitivity to numerical resolution appears to be less than the variability of some of the other unknowns (mass, density, strength, etc.). Nevertheless, to reduce this sensitivity as much as possible further research into numerical resolution sensitivity is being performed.

FIREBALL EVOLUTION

Three-dimensional, bilaterally symmetric simulations most accurately render fireball evolution beginning about 10-15 seconds after first contact of the fragment with Jupiter's atmosphere. We take the results from the two-dimensional entry, deformation and breakup studies, incline them at 45° and map them into a three-dimensional representation for studies of fireball evolution. Density, temperature, fluid velocity and pressure of the cometary debris and shocked Jovian atmospheric constituents are preserved in a spatially average sense while total energy is conserved. The calculation is started and allowed to evolve for up to 120 seconds. Generally, the simulation results indicate that early-time fireball growth is predominantly directed outward along the incoming bolide trajectory but is redirected, at later time, towards growth dominated by the vertical gradient of the Jovian atmosphere.

In order to attain adequate resolution for these large fireball simulations, we performed the calculations on the 1840-processor Intel Paragon massively parallel supercomputer at Sandia National Laboratories. The simulation of the fireball formed by the impact of a 3-km comet fragment consisted of 8 million 5-km cubical zones. Lower energy events, formed by the impact of 1- or 2-km fragments, are modeled with more finely resolved, but less spatially extensive, simulations. Zoning studies that we have performed indicate that, large as these simulations are, they underresolve the shock width and underestimate the temperature of the shock wave that forms in the upper reaches of the Jovian atmosphere. The observability of the shock wave is controversial. Zahnle and Mac Low [17] maintain that the shock wave (formed by a 1-km impactor) in clean Jovian air will be transparent. We note the possibility of contaminating cometary debris from previous impacts and the possibility of non-equilibrium states excited by the shock wave that may make the shock visible [5]. As of September, 1994, no observations of shock waves have been reported, although precursor events were seen by some observers. Because of these issues, our estimates of fireball luminosity do not include potential contributions from the shock front.

The final results from 1- and 3-km fragment impact and fireball simulations are shown in Figure 5. The fragments deposited (as internal energy of H_2, He and H_2O vapor) more than 95% of their kinetic energy (0.2 and 6 million megatons, respectively) during their penetration of the Jovian atmosphere (a comparatively small amount remains as kinetic energy of cometary water vapor). The fireball and surrounding shock wave resulting from a 3 km impactor are shown about 15, 50, and 69 seconds after impact. At 15 seconds, the comet has penetrated to its maximum depth, well below the outermost visible cloud

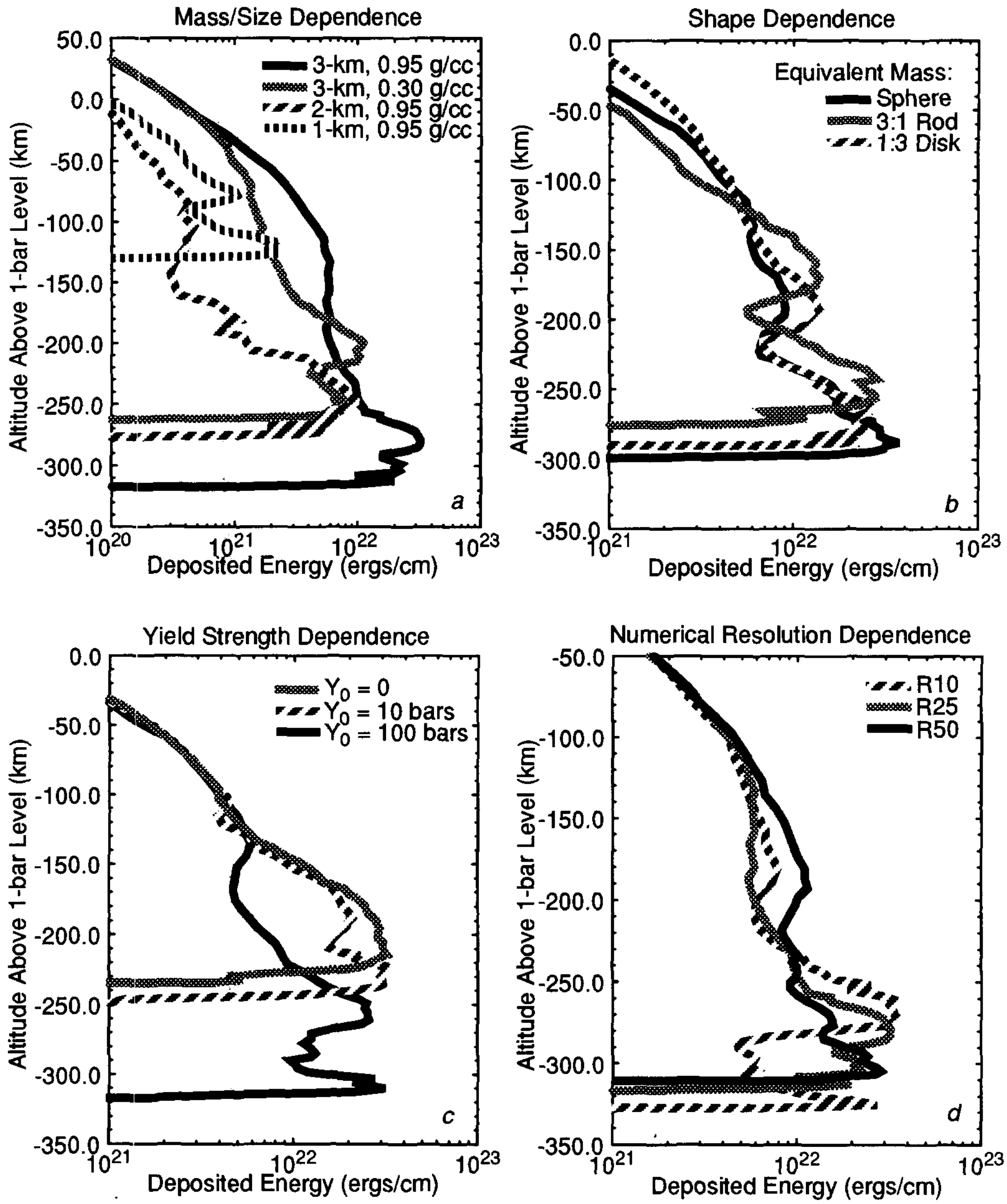

Fig. 4. Energy deposited by hypothetical cometary fragments during their penetration of the Jovian atmosphere. The fragments are modeled as water ice initially traveling at close to escape velocity, 60 km/s. The plots were produced at the end of each numerical simulation by summing the total energy contained within discrete altitude bands (3-25 km thickness) of the computational mesh and normalizing by band thickness. The internal energy contribution of the initial atmosphere has been removed. *a) Mass/Size dependence:* comparison of four R25 penetration simulations. Projectiles consist of 1-, 2- and 3-km fully-dense, strengthless, ice spheres and a porous 3-km ice sphere (mass equivalent to a 2-km fully dense ice sphere). *b) Shape dependence:* comparison of three R25 strengthless ice penetration simulations with equivalent mass sphere, L/D=3 short rod and L/D=0.33 flat disk. *c) Yield strength dependence:* comparison of three R25, L/D=1 ice cylinder penetration simulations with yield strengths of 0, 10 and 100 bars. *d) Numerical resolution dependence:* comparison of three strengthless ice sphere penetrations simulations with resolutions of 10, 25 and 50 zones across the projectile radius.

tops of Jupiter's atmosphere, leaving behind it a trail of hot, high-pressure air and cometary debris which expands explosively into the surrounding atmosphere. This creates a fireball that grows supersonically upwards, initially along the entry path. After 50 seconds, a spherical shock wave can be seen separating from the fireball. It is accelerating upwards at 10 km/sec and has reached a diameter of 300 km and an altitude of 450 km above the Jovian cloud tops. At 69 seconds, the spherical shock wave is advancing upward at a velocity of 25 km/s. It has reached a diameter of 700 km and an altitude of 900 km above the clouds. For reference, the Jovian cloud tops are located at an altitude of 10-20 km and the limb of Jupiter (as seen from Earth) varies as a function of impact location. The limb position for impacts occurring 4 and 6 degrees beyond the limb are at 200 and 400 km altitude, respectively. As of September, 1994, Chodas and Yeomans (unpublished data, 1994) estimated the impact locations ranged from about 4° to about 9° beyond the limb.

The fireball itself is a rapidly rising cloud of cometary debris and Jovian atmosphere at high temperature. Sixty-nine seconds after the impact of a 3-km cometary fragment, the fireball is still at 1700 K, and the shock wave temperature is 2300 K. If the fireball is optically thick, its apparent bolometric magnitude (as viewed from earth) would be about 2 at this time (its bolometric luminosity is $L = 4 \times 10^{23}$ ergs/s, with a blackbody spectrum peaking in the infrared at $\lambda_{max} = 1.7$ μm). This estimate assumes the following: the light is from the visible part of a fireball generated by a 3-km diameter icy impactor 69 seconds after impact, the impact location is a nominal 6° beyond the limb, the fireball is optically thick, and there is no contribution from the high-temperature shock wave. Impacts close to the limb reveal more of the fireball for a brighter magnitude (a 3-km impact 4° beyond the limb yields $L = 10^{24}$ ergs/s, $\lambda_{max} = 1.2$ μm). The fireballs from small, 1-km impactors far from the limb do not appear over the limb until the impact site rotates into view whereas those close to the limb appear dimly ($L = 10^{21}$-10^{22} ergs/s, $\lambda_{max} = 1.3$-1.5 μm) but cool and fade rapidly.

We are calling this hot debris cloud a fireball, but the differences between it and other closely-related phenomena should be outlined. Analogies to the fireball associated with the detonation of a nuclear device are limited. The development of a nuclear fireball is dominated by interior radiative transport at temperatures of tens of millions of degrees. Some fraction of this energy forms a shock wave in the atmosphere, which separates from the fireball but can still be luminous if strong enough. The shock wave generated by the impact fireball is similar to the outer, mechanically-driven nuclear blast wave, but the temperature of the impact-generated shock wave is higher at a given propagation distance because the energy source is about six orders of magnitude greater than a megaton-scale nuclear device. The fireball itself is a ballistically-rising mixture of shocked atmosphere and vaporized cometary material. A nuclear fireball that is small compared to the scale height of the atmosphere will be driven upwards by buoyant forces because it is less dense than the surrounding atmosphere. A large impact fireball can be much greater than the scale height of the Jovian atmosphere. Because the atmospheric pressure is much greater at the bottom than at the top, it is contained at depth and relatively uncontained at altitude. It, therefore, accelerates upwards as if shot from a gun. Even though its density is much greater than the surrounding atmosphere at the top, its inertia will carry it on a ballistic trajectory which rises as much as several thousand kilometers above the clouds.

OBSERVABLES

Most of the simulations presented here were performed before the impacts took place on Jupiter and are documented elsewhere [4-7]. The principle scientific reason for simulating this event before it happened was to make predictions that could guide observers to collect useful data. From another perspective, the impact event can be considered a large experiment by which the simulations can be validated on a scale many orders of magnitude beyond that which can be achieved in the laboratory. The simulations are providing insight into the physical mechanisms and instabilities that lead to the breakup of the cometary fragment, transfer of energy and growth of the fireball. Finally, this event is of interest to a wide-ranging community, so it is being analyzed by a variety of numerical and analytical technques [2-20]. These solutions can be used to benchmark, or cross-validate one another.

A particularly useful set of observations that was made by many observers, including the Voyager II, Galileo and Ulysses spacecraft, were the light curves produced by each of the large impact/fireball events as functions of time. As has been noted by many workers, the entry of each cometary fragment into the Jovian atmosphere produces a burst of light before the fragment penetrates below the visible cloud tops and disappears from view. Our simulations show that the deposition of the fragment's kinetic energy along

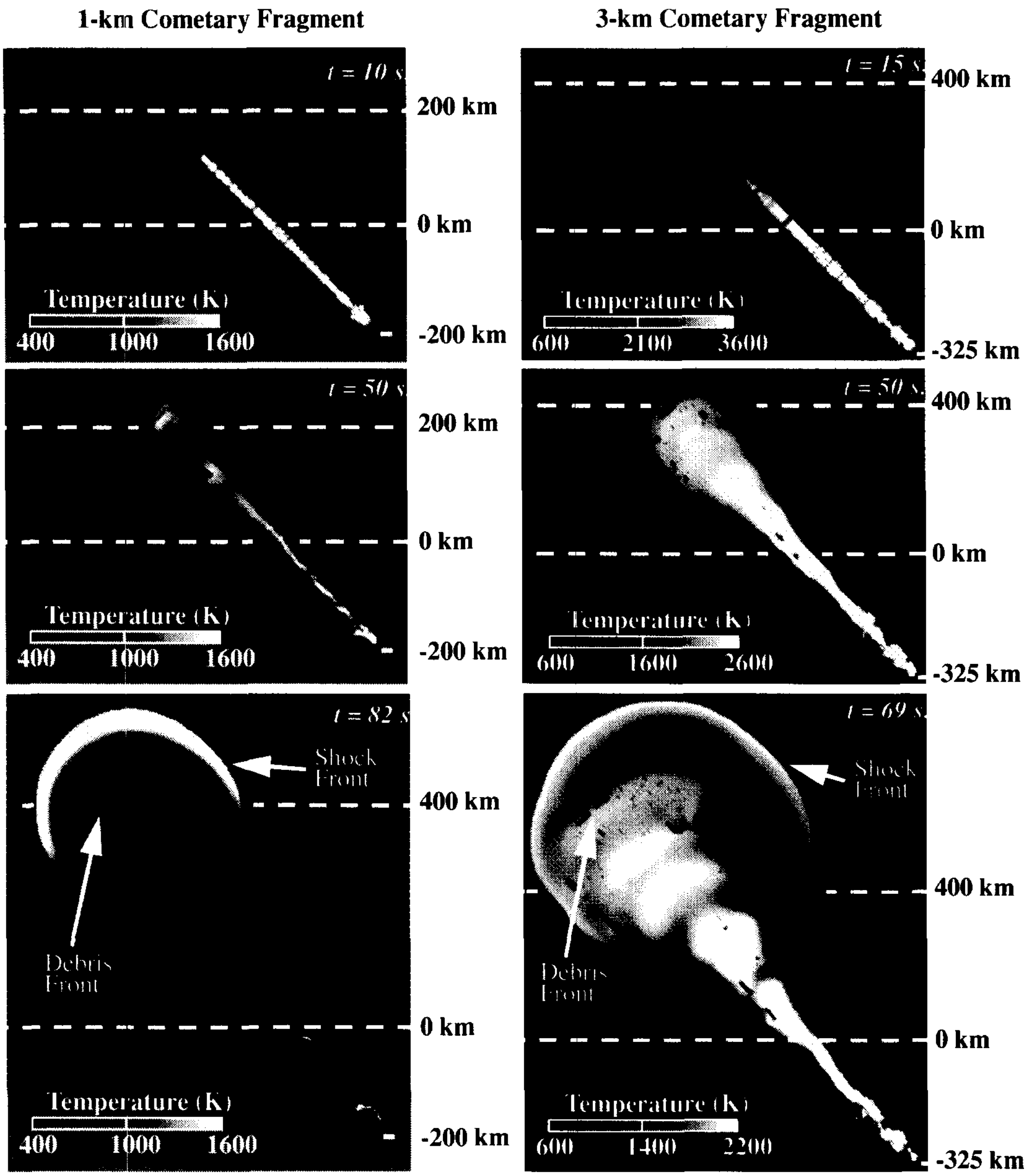

Fig 5. Fireball formed by the impact of 1 and 3 km fragments of Comet Shoemaker-Levy 9 on Jupiter (cross-sectional view with temperature represented by grayscale). The fragments deposited most of their kinetic energy into the atmosphere in the first 10-15 seconds (the 2-D simulations of Fig. 3). The fireballs shown here are the result of that tremendous energy deposition. Late in the simulation, a shock front has discernably detached from a debris front, consisting of cometary debris (water vapor) and shock-heated atmospheric gases (H_2 and He), Material in the debris front, originally left in the wake of the entering cometary fragment below 100 km altitude, has been entrained and uplifted by the fireball to altitudes great enough to be in line-of-sight with Earth as early as 20-30 seconds after some of the impacts (see text for further description).

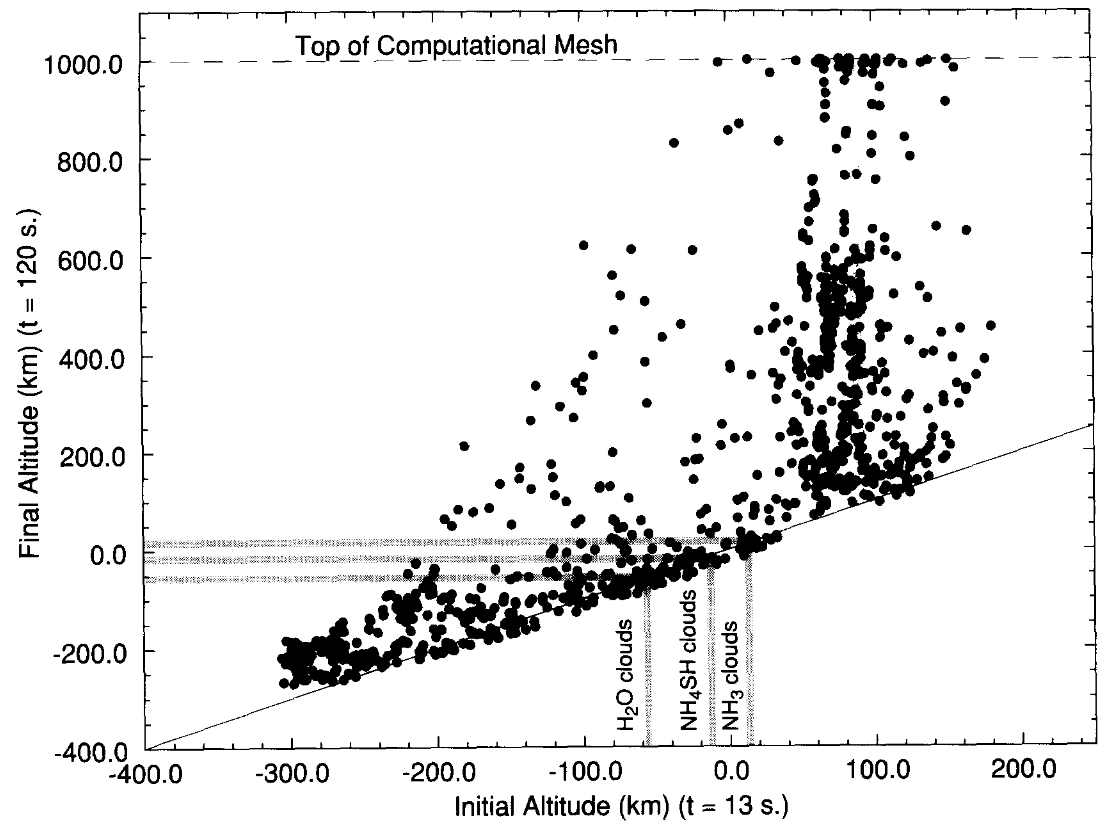

Fig. 6. Final altitude (t = 120 s.) vs. initial altitude (t = 13 s.) for 998 Lagrangian tracer particles distributed on an equal volume basis throughout the fireball generated from the impact of a 3-km fragment. This late in the calculation, some of the fireball material has reached the top of the computational mesh (shown by the dashed line). Any particle plotted on the solid line, which has a slope of 1:1, has had no net change in altitude over this time period.

its entry path within the atmosphere leads to the development of a fireball that grows upwards and outwards at a rate dependent on the original fragment mass and size. For a nominal impact occurring 6° beyond Jupiter's limb, minimum altitude of direct earth line-of-sight is about 400 km above the 1-bar level. Our simulation of a 3-km ice body predicts that the time interval between fragment entry and fireball arrival into line-of-sight from Earth is between 45 and 50 seconds under these circumstances. Results from simulations of smaller-body impacts indicate that the time interval in these cases is substantially increased. Because the observed limb of the planet is dependent on the wavelength of light used to make the observations, multiple points on the fireball trajectory can be determined from observations that used different filters.

To estimate the origin and final distribution of the material incoporated in the fireball, we followed 998 Lagrangian tracer particles throughout the duration of the simulation. The particles were distributed randomly on an equal volume basis. Approximately half represent cometary material and half represent Jovian atmosphere. Figure 6 shows the initial and final altitudes of the tracer particles after two minutes of fireball evolution. While some of the particles have piled up at the top of the computational mesh, it is evident that the bulk of the upper fireball volume is derived from relatively high altitude Jovian atmospheric materials. By summing over the mass of each particle we estimate the total fireball mass above the 1-bar level as 9.5 x 10^{16} g (6.8 fragment masses). Less than 0.2% (1.7 x 10^{14} g) of the fireball above the 1-bar level is made up of impactor material; most of the fragment's mass stays deep within the atmosphere. Moreover, the simulations show that the mass density of the fireball has a strong dependence on altitude. Only 1.9 x 10^{15} g (0.14 fragment masses) of the fireball mass is above the 400 km level with 9.0 x 10^{14} g of this derived from material below the -60 km level (the approximate level below which water may be relatively abundant in the Jovian atmosphere) and 2.5 x 10^{13} g derived from cometary material.

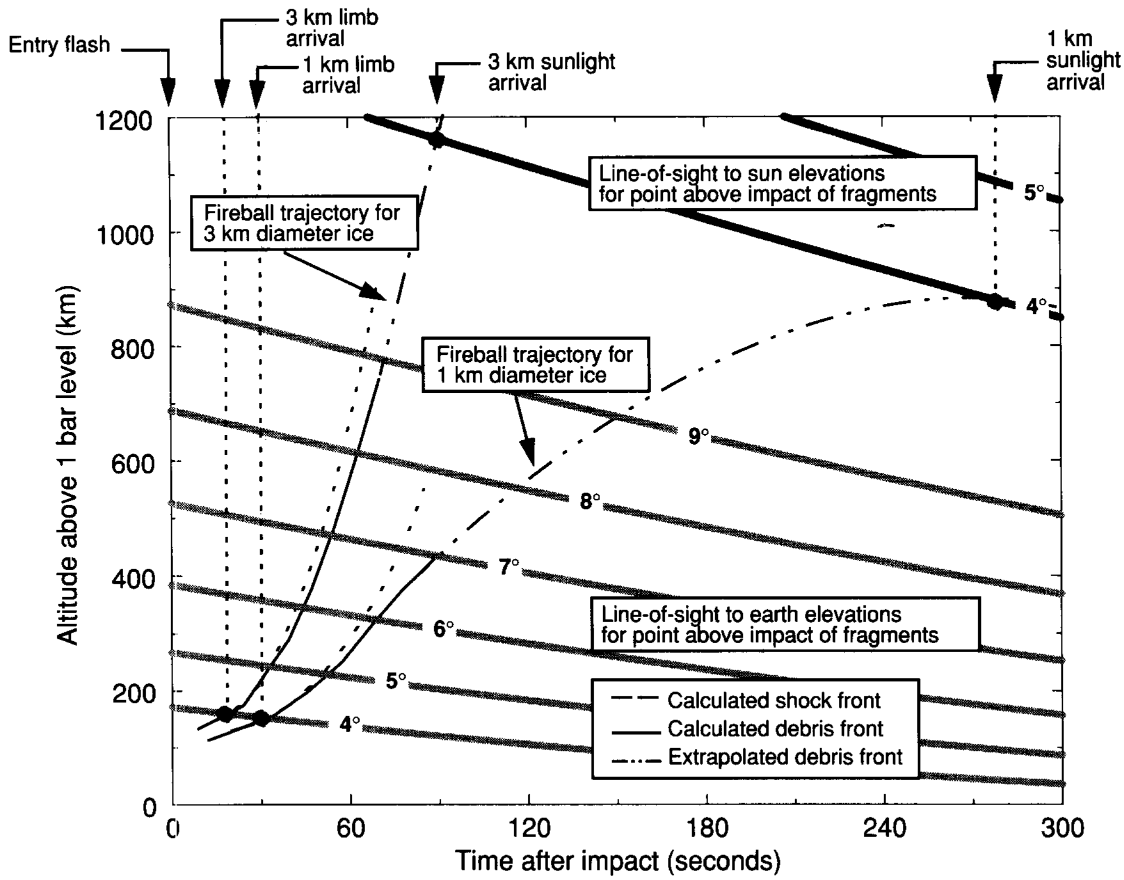

Fig. 7. Calculated trajectories of shock front and debris front (fireball) from three dimensional PCTH simulations for 1- and 3-km diameter ice fragments. Approximate line-of-sight elevations to the Earth (light shading) and to the sun (dark shading) for selected impact locations (identified by angle over the limb at time of impact) allow potentially observable arrival times to be estimated. The debris front is ballistically extrapolated beyond the end of the simulations. Modified from [6].

The geometry of impact is shown in Figure 1. Because the dawn terminator is about 7° from the limb, the line-of-sight to the sun is significantly higher above the point of impact, so that when the fireball (observable in the infrared) rises above the limb, it is not, initially, in sunlight. If the fireball is moving fast enough (as it is for impacts of 1-km objects) it continues to rise until it is illuminated by the sun a few minutes after impact. This event is observable if the fireball is dense enough to scatter sunlight. Of course the fireballs from smaller impacts enter sunlight once the impact sites rotate into view 10-30 minutes later. The strong infrared emission seen by many Earth-based observers for many hours after impact was probably due to the re-entry of fireball material which heated broad regions of the stratosphere and upper troposphere. Generally, this material re-enters the atmosphere at a velocity of 10-20 km/s and is capable of producing the strong thermal signatures that were seen.

Figure 7 shows fireball trajectories determined by our 3-D PCTH simulations for 1 and 3 km impactors, with fireball altitudes plotted as a function of time after impact. Also plotted are line-of-sight elevations from the earth (lightly shaded curves) and the sun (darker curves) for selected impactors (which are identified by their letter designations). These elevations were determined using the projected impact locations of Chodas and Yeomans (unpublished data, 1994). As the impact points rotate toward the limb, the line-of-sight elevations move lower; so these curves decrease with time after impact. This diagram shows how, for a given fragment, (assuming a 1- or 3- km diameter) the times of arrival over the limb and into the sunlight can be estimated from our calculated trajectories. Knowledge of this trajectory, when compared to simulations, will allow the mass of the fragments and their approximate depth of penetration to be determined. These estimates can be further refined by comparing the predicted fireball trajectory, morphology and temperature with that determined from high resolution imagery, spectrometry and time-resolved photometry.

ACKNOWLEDGMENTS

This work was supported by the United States Department of Energy under Contract DE-AC04-94AL85000. This material is based upon activities supported by the National Science Foundation under Agreement No. 9322118. Any opinions, findings, and conclusions or recommendations expressed in this publication are those of the authors and do not necessarily reflect the views of the National Science Foundation.

REFERENCES

1. Weaver, H. A., Studying Comet P/Shoemaker Levy 9 with the Hubble Space Telescope. *EOS*, **75**, 225 (1994).
2. Scotti J.V., Melsoh H.J., Tidal breakup and disruption of P/Shoemaker-Levy 9: estimate of progenitor size, *Nature*, **365**, 7333 (1993).
3. Asphaug, E. and Benz, W., Density of comet Shoemaker-Levy 9 deduced by modelling breakup of the parent 'rubble pile', *Nature*, **370**, 120-124 (1994).
4. Crawford, D. A., M. B. Boslough, T. G. Trucano, and A. C. Robinson, The impact of Comet Shoemaker-Levy 9 on Jupiter, *Shock Waves*, **4**, 47-50 (1994).
5. Boslough, M. B., D. A. Crawford, T. G. Trucano, and A. C. Robinson, Mass and penetration depth of Shoemaker-Levy 9 fragments from time-resolved photometry, *Geophys. Res. Lett.*, **21**, 1555-1558 (1994).
6. Boslough, M. B., D. A. Crawford, T. G. Trucano, and A. C. Robinson, Watching for Fireballs on Jupiter, *EOS*, **75**, 305 (1994).
7. Crawford, D. A., T. G. Trucano, M. B. Boslough, M. E. Kipp and J. M. McGlaun, The Influence of Body Shape on the Deformation and Breakup of Comet Shoemaker-Levy 9 Fragments as They Enter the Jovian Atmosphere, *Lunar and Planet. Sci.* **25**, 295-296 (1994).
8. Hills J.G., Goda M.P., The fragmentation of small asteroids in the atmosphere, Astron. J. **105**, 1114-1144 (1993).
9. Moran, B. and R. Tipton, Simulation of a comet impact on Jupiter. *EOS*, **74**, 389 (1993).
10. Sekanina, Z., Disintegration phenomena expected during the forthcoming collision of periodic comet Shoemaker-Levy 9 with Jupiter. *Science* **262**, 382 (1993).
11. Vickery, A., Numerical simulation of a comet impact on Jupiter. *EOS*, **74**, 391 (1993).
12. Ivanov, B. A. and H. J. Melosh, Dynamic fragmentation of a comet in the Jovian atmosphere, *Lunar and Planet. Sci.* **25**, 597-598 (1994).
13. Mac Low, M.-M. and K. Zahnle, Explosion of Comet Shoemaker-Levy 9 on entry into the Jovian atmosphere, *Astophysical Journal Letters*, in press (1994).
14. Takata, T., J. D. O'Keefe, T. J. Ahrens and G. S. Orton, Comet Shoemaker-Levy-9: impact on Jupiter and plume evolution. *Icarus*, **109**, 3-19 (1994).
15. Ahrens, T. J., T. Takata, J. D. O'Keefe and G. S. Orton, Impact of Comet Shoemaker-Levy 9 on Jupiter, *Geophys. Res. Letts.*, **21**, 1087-1090 (1994).
16. Ahrens, T. J., T. Takata, J. D. O'Keefe and G. S. Orton, Radiative signatures from impact of Comet Shoemaker-Levy-9 on Jupiter, *Geophys. Res. Letts.*, **21**, 1551-1553 (1994).
17. Zahnle K. and Mac Low M.-M., The Collision of Jupiter and Comet Shoemaker-Levy 9, *Icarus*, in press, (1994).
18. Harrington, J., R. P. LeBeau Jr., K. A. Backes, and T. E. Dowling, Dynamic response of Jupiter's atmosphere to the impact of comet Shoemaker-Levy 9, *Nature*, **386**, 525 (1994).
19. Ingersoll, A. P., H. Kanamori, and T. E. Dowling, Atmospheric gravity waves from the impact of comet Shoemaker-Levy 9 with Jupiter, *Geophys. Res. Lett.* **21**, 1083-1086 (1994).
20. Marley, M. S., Seismological consequences of the collision of comet Shoemaker-Levy/9 with Jupiter, *Astrophys. J. Lett*, in press (1994).
21. McGlaun, J. M., S. L. Thompson and M. G. Elrick, CTH- A three-dimensional shock-wave physics code, *Int. J. Impact Engng.*, **10**, 351 (1990).
22. Thompson, S. L., ANEOS analytic equations of state for shock physics codes input manual, Sandia National Laboratories, SAND89-2951 (1989).
23. Kerley, G. I., User's manual for PANDA II: a computer code for calculating equations of state, Sandia National Laboratories, SAND88-2291 (1991).
24. Swegle, J. W. and A. C. Robinson, Accleration instability in elastic-plastic solids. I. Numerical simulations of plate acceleration, *J. Appl. Phys.* **66**, 2838 (1989).